Research Paper

Influence of the halide and exposed facets on the visible-light photoactivity of bismuth oxyhalides for selective aerobic oxidation of primary amines

Aijuan Han[*], Hongwei Zhang, Gaik-Khuan Chuah[*], Stephan Jaenicke

Department of Chemistry, National University of Singapore, 3 Science Drive, Singapore 117543, Singapore

ABSTRACT

Bismuth oxyhalides BiOX (X = Cl, Br, I) are seldom applied as photocatalysts in organic synthesis. Herein, we investigated their potential for the aerobic oxidative coupling of benzylamine to *N*-benzylidenebenzylamine, as imines are important synthetic intermediates of pharmaceuticals and biologically active nitrogen-containing organic compounds. The influence of the halide and the exposed crystal facets on the photoactivity was investigated. BiOBr showed excellent photoactivity, surpassing BiOCl and BiOI, which have poor light absorption and oxidation ability, respectively. Three differently facetted BiOBr photocatalysts were synthesized. The {001}-facetted BiOBr exhibited higher intrinsic activity than the {010}- or {110}-samples due to efficient charge separation. However, surface area plays an important role as reactions usually occur at the catalyst surface. Because of their much larger surface area, the solvothermally-synthesized BiOBr microspheres with {110}-dominant exposed facet showed the highest photooxidative activity, with 100% conversion and 100% selectivity to *N*-benzylidenebenzylamine after 14 h visible light irradiation at room temperature using oxygen from atmospheric air. This work provides an economical, feasible, sustainable and green process for the synthesis of imines and illustrates the great potential of bismuth oxyhalides as photocatalysts for organic synthesis.

© 2017 Elsevier B.V. All rights reserved.

1. Introduction

Imines are important synthetic intermediates of pharmaceuticals and biologically active nitrogen-containing organic compounds [1,2]. Traditionally, the synthesis of secondary imines involves condensation of primary amines with carbonyl compounds (mostly aldehydes) followed by dehydration (Scheme 1, reaction 1) [3,4]. However, aldehydes are extremely reactive and not easy to handle. Following environmental-benign concepts, the direct oxidation of primary amines to secondary imines using molecular oxygen (Scheme 1, reaction 2) will be a superior method. Ruthenium and gold-based catalysts, such as RuCl₃ [5], Ru-porphyrin [6], Ru/Al₂O₃ [7], Au/Al₂O₃ [8], Au/CeO₂ [9], and Au/graphite [10], have been found to be active for this reaction. Despite the use of precious metals, high temperature, typically > 100 °C, is required for the reaction. Very recently, photocata-

lysts such as TiO₂ [11], (Zn^II/Ti^IV) layered double hydroxide [12], and Nb₂O₅ [13], have been reported to catalyse the conversion of amines into imines at low temperatures with the assistance of UV light.

Visible light is more readily available than the higher energy UV radiation and research increasingly focuses on visible-light active photocatalysts. Mesoporous-C₃N₄ [14], CdS [15], Au-Pd/ZrO₂ [16], conjugated microporous poly(benzooxadiazole) networks [17], and hollow microporous organic networks [18] have been reported as active and highly selective catalysts for this reaction (≥99%). However, pure oxygen at high pressure is required, which translates into higher costs and increases the safety concerns for larger-scale production. To date, only Au/TiO₂ [19] and BiVO₄ together with a copper complex [20] can achieve 99% selectivity using atmospheric air as the oxygen source for benzylamine oxidation into secondary imines under visible light. However, for the former, a precious metal is necessary, which will add to the material cost while metal leaching during the reaction makes it difficult to reuse the catalyst. In the other example, an expensive and non-reusable copper complex has to be added together with BiVO₄ which poses problems in the product isolation. There-
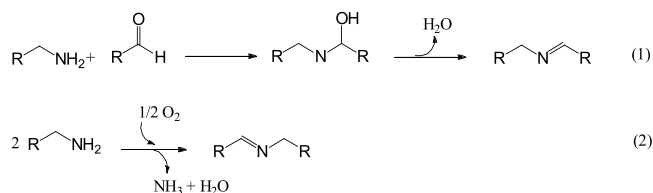
Scheme 1. Two ways for the formation of secondary imines.

fore, developing environmentally benign materials that work under mild conditions (atmospheric air and low temperature) with high selectivity remains a big challenge in this area.

Although bismuth is a heavy metal, it is considered as an environmental friendly element and its compounds are widely used in pharmaceuticals and cosmetics [21,22]. Bismuth compounds, such as BiOX [23–28], BiVO$_4$ [29,30], Bi$_2$WO$_6$ [31,32] and Bi$_2$O$_3$ [33,34] have been intensively studied as photocatalysts for pollutant remediation and hydrogen production. Especially the bismuth oxyhalides BiOX (X = F, Cl, Br, I) which crystallize in a tetragonal structure with alternating layers of [Bi$_2$O$_2$]$^{2+}$ and negatively charged halogen ions have drawn much attention in water remediation and water splitting. However, research into their applications in organic synthesis is sparse. To the best of our knowledge, there is no report about bismuth oxyhalide for the photocatalytic oxidative coupling of primary amines to the corresponding imines.

In the present work, we synthesized BiOX (X = Cl, Br, and I) microspheres composed of nanosheets with different halides as well as BiOBr nanosheets with different exposed facets, i.e. (110), (001) and (010), and investigated their application as visible-light photocatalysts in the selective oxidation of benzylamine to N-benzylidenebenzylamine. It was found that both the halide and the exposed facets critically influence the catalytic activity. BiOBr microspheres, composed of nanosheets with (110) dominated facet, can catalyse the selective oxidation of benzylamine to N-benzylidenebenzylamine to realize a 100% conversion and 100% selectivity after 14 h visible light irradiation using atmospheric air at room temperature. The present work offers an easy-handling, economical, sustainable, and green process for the synthesis of imines and sheds light on the great potential of bismuth oxyhalides as photocatalysts for organic synthesis.

2. Experimental

2.1. Synthesis of BiOX

BiOX (X = Cl, Br, I) were synthesized by a solvothermal method. In a typical synthesis, solution A was prepared by dissolving 2 mmol of Bi(NO$_3$)$_3$·5H$_2$O in 10 ml of dimethylformamide (DMF) and methanol (5:5), while solution B contained 2 mmol of NaCl (or KBr, KI) in 0.1 ml H$_2$O, 5 ml DMF and 5 ml methanol. Solution B was added into solution A and after stirring for 30 min, the mixture was poured into a 40 ml Teflon-lined stainless steel autoclave and kept at 130 °C for 2 h under autogenous pressure. The resulting precipitate was collected by centrifugation, washed with absolute ethanol, and dried overnight in an oven at 80 °C. These samples are labelled as BiOX-S.

BiOBr exposing predominantly (001) facets (BiOBr-001) or (010) facets (BiOBr-010) were synthesized by pH variation following earlier literature [26]. Under acidic synthesis conditions, adsorption of H$^+$ ions at the O-terminated (001) surface hinders growth in the [001] direction and therefore leads to the preferential formation of (001) facetted planes. At a higher pH of 6, the growth of other planes is favoured. For {010}-facetted BiOBr (denoted as BiOBr-010), 2 mmol Bi(NO$_3$)$_3$·5H$_2$O and 6 mmol of KBr were dissolved in 30 ml of deionized water and the pH was adjusted to 6 by addition of 2 M NaOH. After stirring for 15 min, the solution was poured into a 40 ml Teflon-lined stainless steel autoclave and kept at 160 °C for 2 h under autogenous pressure. The resulting precipitate was collected by centrifugation, washed with absolute ethanol, and dried in an oven at 80 °C overnight. The sample prepared without adding any NaOH had a pH of 2.3 and was denoted as BiOBr-001.

2.2. Characterization

Powder X-ray diffraction patterns were measured with a Siemens D5005 diffractometer using Cu K$_\alpha$ radiation. The 2θ angle from 5 to 80° was scanned at 0.02°/s with a dwell time of 1 s/step. Nitrogen adsorption and desorption isotherms were measured at 77 K with a porosimeter (TriStar 3000, Micromeritics). The Brunauer-Emmett-Teller equation was used to calculate the specific surface area. Scanning electron microscopy (SEM) was performed on a JEOL JSM-6701F SEM (field-emission) microscope with 5 kV electron beam energy. Transmission electron micrographs were obtained with a JEOL 3010 operated at 200 kV. UV–vis diffuse reflectance spectra were measured with a Shimadzu UV-2450 UV–vis spectrophotometer. The adsorption of benzylamine on the samples was measured by equilibrating 100 mg BiOBr in various concentrations of benzylamine in acetonitrile (0.0025–0.04 M). Adsorption was carried out in the dark for 24 h and the benzylamine remaining in solution was determined by UV spectroscopy.

2.3. Photocatalytic activity

The photocatalytic amine oxidation was performed in an open glass tube (Fig. S1b) to allow access to atmospheric air for the continuous supply of oxygen. About 100 mg photocatalyst was suspended in 5 ml acetonitrile containing 0.1 mmol benzylamine. The sample was placed in a water bath at room temperature and irradiated with a 15 W Philips fluorescent lamp (λ ∼ 400–650 nm) placed at a distance of 2.5 cm from the side of the tube. At regular time intervals, about 0.2 ml aliquots were removed and filtered through a syringe filter. The filtrates were analyzed by a gas chromatograph (HP 6890N) equipped with a HP-5 column and a FID detector. The identity of the peaks was confirmed by gas chromatography mass spectrometry (Shimadzu GCMS-QP5000). The conversion and selectivity were calculated based on the peak areas of the starting materials and all products including by-products.

A blank experiment was conducted under the same condition with only 5 ml acetonitrile in the glass tube to estimate the amount of solvent evaporation. Less than 3% of the solvent evaporated over the course of a 14 h experiment (Fig. S1), assuring that solvent evaporation did not significantly influence the results.

3. Results and discussion

3.1. Characterization

The BiOX samples were crystalline and their diffraction patterns fitted well with the corresponding tetragonal BiOX structures (BiOCl JCPDS No. 06-0249, BiOBr JCPDS No.09-0393, BiOI JCPDS No. 10-0045), respectively (Figs. 1 and S2). No extra peaks were found, showing the high purity of the samples. From scanning electron microscopy, the BiOX-S samples prepared by the solvothermal method are composed of nanosheets with thickness of ∼ 30 nm aggregated into microspheres of 2–7 μm size (Fig. 2a–c). In contrast, BiOBr-001 and BiOBr-010 which were prepared without using organic solvents formed platelets but did not aggregate into microspheres (Fig. 2d & e). These platelets were bigger than those formed by the solvothermal synthesis. Their sizes are in the range of 0.5–3 μm with thickness of 100–200 nm for BiOBr-001 and 50–100 nm for BiOBr-010.
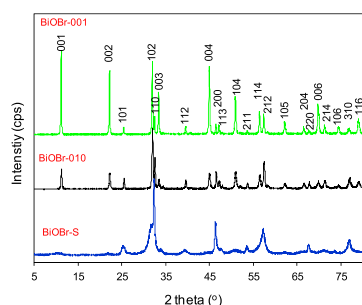
Fig. 1. XRD of BiOBr-S, BiOBr-001 and BiOBr-010.

Table 1
Physical properties of BiOX samples.

Catalyst	Surf. Area (m^2 g^{-1})	Band Gap (eV)
BiOCl-S	30.3	3.54
BiOBr-S	19.1	2.92
BiOBr-001	2.4	2.88
BiOBr-010	6.2	2.90
BiOI-S	15.7	1.92

The high resolution transmission electron micrographs of BiOBr-S exhibited clear lattice fringes with an interplanar lattice spacing of 0.28 nm, corresponding to the ($\bar{1}$10) plane (Fig. 2f). In the selected area electron diffraction patterns, the labelled angle of 46° is in good agreement with the theoretical value between the ($\bar{1}$10) and ($\bar{1}$13) plane for the tetragonal symmetry group. Hence, the diffraction spots can be indexed to the [110] zone axis. This shows that {110} facets dominate in the nanosheets of BiOBr-S, which is consistent with the XRD results where the (110) peak at 32.4° is the most intense peak. Similarly, the dominant exposed facets of BiOBr-001 and BiOBr-010 were deduced from TEM to be {001} and {010}, respectively (Fig. S3).

The solvothermally synthesized BiOX-S samples had higher surface areas in the range of 15.7 m^2/g to 30.3 m^2/g (Table 1). This can be attributed to their hierarchical morphology. In contrast, BiOBr-001 with the larger and thicker platelets has a much lower surface
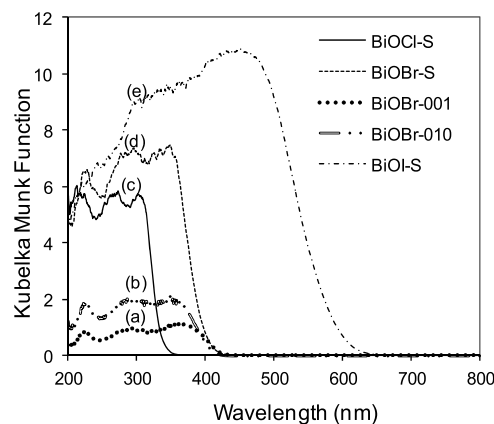

Fig. 3. UV-vis spectra of (a) BiOBr-001, (b) BiOBr-010, (c) BiOCl-S, (d) BiOBr-S and (e) BiOI-S.

area of only 2.4 m^2/g. BiOBr-010 with large but thinner platelets has a higher surface area of 6.2 m^2/g.

The absorption spectra obtained by Kubelka-Munk transformation of the diffuse UV reflectance spectra of BiOCl-S show no absorption in the visible region while BiOBr-S and BiOI-S absorb in the visible range up to 420 nm and 620 nm, respectively (Fig. 3). For BiOBr, the absorption edge positions are similar for the three differently synthesized samples. They differ only in the absorption intensity with BiOBr-S having much higher absorption than the facetted BiOBr-010 or BiOBr-001. This may be due to the higher surface area and unique hierarchical structure of the former which facilitates multiple light reflections. The band gap was calculated from a Tauc plot, of $(F(R_\infty) \cdot h\nu)^{1/\eta}$ versus $h\nu$ where BaSO$_4$ is used as a reference, ν = light frequency, and η = 2 for an indirect transition (Fig. S4 and Table 1) [35]. The band gap increases from 1.92 in BiOI to 3.54 eV for BiOCl.

3.2. Photocatalytic activity

The photocatalytic oxidation of benzylamine was carried out at room temperature with atmospheric air as the oxidizing agent.
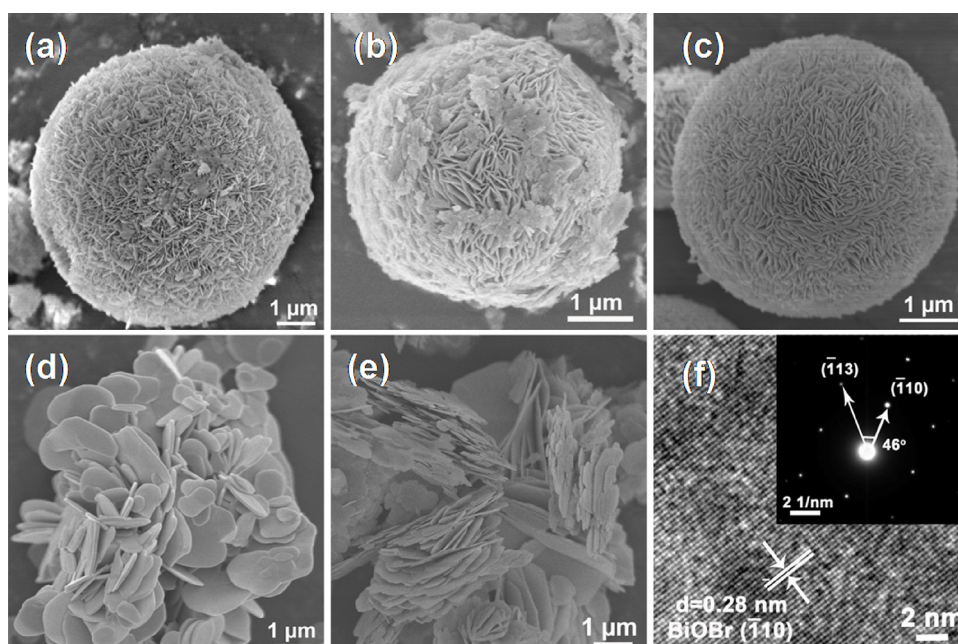

Fig. 2. SEM images of (a) BiOCl-S, (b) BiOI-S, (c) BiOBr-S, (d) BiOBr-001, (e) BiOBr-010 and (f) HRTEM image of BiOBr-S (insert: selected area electron diffraction).

Table 2
Benzylamine oxidation in the presence of different catalysts.

Entry	Catalyst	Solvent	Time (h)	Conv. (%)	Sel. (%)
1	no catalyst	ACN	14	0.8	–
2	BiOCl-S	ACN	14	69.6	98.3
3	BiOI-S	ACN	14	50.7	100
4	BiOBr-S-110	ACN	14	100	100
5[a]	BiOBr-S-110	ACN	14	0	–
6	BiOBr-S-110	toluene	14	98.0	100
7	BiOBr-S-110	H$_2$O	14	18.5	100
8	BiOBr-S-110	methanol	14	100	26.1
9	BiOBr-S-110	DMF	14	100	100
10	BiOBr-S-110	dimethyl carbonate	14	96.4	91.9
11[b]	BiOBr-S-110	ACN	6	100	100
12[c]	BiOBr-S-110	ACN	5	100	100
13	BiOBr-001	ACN	14	87.1	100
14	BiOBr-010	ACN	14	43.1	100
15[d]	–	ACN	14	9.6	100
16[e]	BiOBr-S-110	ACN	100	100	97.0

Reaction condition: 0.1 mmol benzylamine, 100 mg catalyst, 5 ml solvent, 15 W Philips compact fluorescent lamp, 14 h, 25 °C.

Essentially no reaction took place in the absence of catalyst (Table 2, entry 1) which indicates that benzylamine is stable under visible light irradiation. The most active photocatalyst in the group of solvothermally prepared bismuth oxyhalides was BiOBr-S which gave 100% conversion after 14 h (Table 2, entry 4 and Fig. S5). The conversion was only 69% and 51% with BiOCl-S and BiOI-S, respectively (Table 2, entry 2–3). With all the catalysts, the selectivity to N-benzylidenebenzylamine was very high, 98 − 100%. The only other product formed was benzylimine. To the best of our knowledge, this is the first non-noble metal-containing photocatalyst that achieves such a good performance under visible light irradiation at room temperature with atmospheric oxygen (Table S1). Furthermore, bismuth is earth abundant and can be considered as environmentally friendly. These properties are advantageous for its practical application. No reaction occurred when there was no light irradiation, indicating that the aerobic oxidation of benzylamine is indeed a photocatalytic process.

Using BiOBr-S as the photocatalyst, different solvents were investigated (Table 2, entry 4, 6–10). In water, only 18.5% conversion could be observed after 14 h although the desired product, N-benzylidenebenzylamine, was formed with 100% selectivity. In methanol, the conversion was 100% after the same time, but the selectivity was only 26.1%. In dimethyl carbonate, a green solvent, the conversion was 96.4% whereas the selectivity was 91.9%, limiting its usage due to the noticeable amount of by-product. In DMF, toluene and acetonitrile, conversion and selectivity were both high. Acetonitrile is the preferred solvent because its low boiling point of 81 °C facilitates its later separation from the product for recycle in

another run under practical applications (Table S2). It was therefore used for all subsequent photocatalytic studies. At room temperature, the reaction was accomplished with 100% conversion and 100% selectivity after 14 h. Under higher reaction temperatures, the reaction was accelerated without the yield being sacrificed. 100% yield was achieved after 6 h and 5 h for 40 °C and 60 °C, respectively. Because of the easier setup and already high yields, room temperature conditions were used for the following catalytic studies. When the benzylamine concentration was increased tenfold to 1 mmol (Table 2 entry 16), 97% yield of N-benzylidenebenzylamine was obtained over BiOBr-S after 100 h.

It is interesting to note that BiOCl was able to photocatalyze the reaction despite its wide band gap of 3.54 eV which means that it can only utilize light <350 nm. A similar observation was made by Higashimoto et al. for the photocatalytic oxidation of benzylamine over TiO$_2$ under visible light [36]. From spectroscopic studies and DFT calculations, these authors postulated the formation of a surface complex between benzylamine and TiO$_2$ which created a new donor level of localized N 2p orbitals above the valence band of TiO$_2$. Hence, excitation of the electrons can occur at a lower energy than the band gap of the material. Although BiOI can absorb more visible light than BiOBr, its photocatalytic activity was lower. This is due to its lower oxidation ability as indicated by the position of the valence band. Using the Mulliken electronegativity of the individual atoms, the valence band position can be calculated as: $E_{VB} = \chi - E^e + (1/2)E_g$ [37]. The valence band position changed from 3.63 eV in BiOCl to 2.40 eV in BiOI, indicating a decrease in the oxidation ability (Fig. S6).
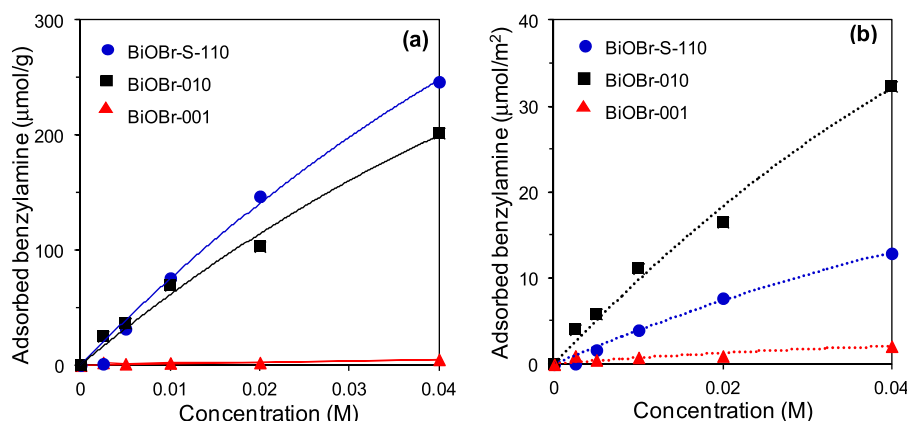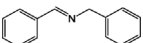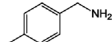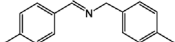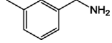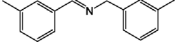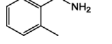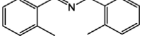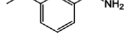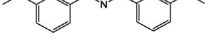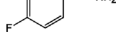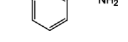

Fig. 4. (a) Adsorption of benzylamine in (a) μmol g^{-1} and (b) μmol m^{-2} for BiOBr-S-110, BiOBr-010 and BiOBr-001.

Table 3
Selective oxidation of various amines over BiOBr-S-110.

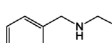| Entry	Amine	Products	Conv. (%)	Sel. (%)
1			100	100
2			93.0	31.9
3			100	100
4			96.9	96.8
5			100	100
6			98.3	15.5
7			100	100
8		–	0	–
9		–	0	–
10			37.0	90.7

Conditions: 0.1 mmol amine, 100 mg catalyst, 5 ml ACN, 15 W Philips lamp, 14 h, 25 °C.

The effect of facetted planes was studied using the most photoactive material, BiOBr. Over BiOBr-010 with dominant {010} planes, the conversion after 14 h reached 43% (Table 2, entry 14). In comparison, the conversion was 87% for the {001}-dominant BiOBr-001 sample although its surface area is only $1/3$ that of the former (Table 2, entry 13). Furthermore, BiOBr-S which has {110}-dominant exposed facets, (henceforth denoted as BiOBr-S-110) was only just slightly more active than BiOBr-001 despite having an 8-fold larger surface area and higher visible light absorption than BiOBr-{001}. These results indicate that the nature of the exposed facet plays an important part in the reaction.

To investigate if the adsorption of benzylamine plays a role, the BiOBr samples were equilibrated in different concentrations of benzylamine in acetonitrile (Fig. 4). The amount adsorbed increased with the surface area, although not proportionally. The enhanced adsorption for BiOBr-010 compared to the other two samples is very apparent when the comparison is based on unit surface area. The specific adsorption of benzylamine (per m^2) decreased in the order of BiOBr-010 > BiOBr-S-110 > BiOBr-001 for all concentrations. For the reaction concentration of 0.02 M, the adsorbed benzylamine was 17 and 7.7 μmoles m^{-2} for BiOBr-010 and BiOBr-S-110, respectively, while only 0.96 μmoles m^{-2} were adsorbed at the surface of BiOBr-001. If benzylamine adsorbs flat at the surface (cross-sectional area 0.7×0.8 nm^2), monolayer coverage would be equivalent to 3.0 μmol m^{-2} while for end-on adsorption via the NH$_2$ group (cross-sectional area of 0.14 nm^2), a monolayer would form at 12 μmol m^{-2}. The enhanced adsorption at the (010) plane, which contains Bi, Br and O (Fig. 5), may be due to interaction between the Lewis basic Bi^{3+} and the nucleophilic nitrogen of benzylamine. Based on Density Functional Theory calculation as implemented in the CASTEP code of the Materials Studio software, the valence band of BiOBr comprised a large contribution from Bi 6p (Fig. S7). Therefore, the adsorption site of benzylamine is where the holes are mainly generated. The strong interaction between benzylamine and BiOBr can facilitate direct hole oxidation of benzylamine. For the (110) plane which has an open structure with rows of oxygen separated by Bi and Br atoms in the second layer, less adsorption was observed. The lowest adsorption was for the (001) plane which has only oxygen atoms at its surface. Neverthe-
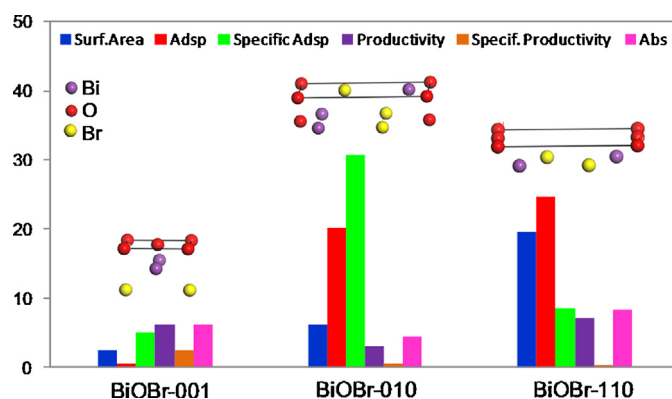

Fig. 5. Surface area (m^2 g^{-1}), adsorption (μmol g^{-1}) and specific adsorption (μmol m^{-2}) of benzylamine, productivity (mmol g$_{cat}^{-1}$ h^{-1}) and specific productivity (mmol m$_{cat}^{-2}$ h^{-1}) of benzylamine oxidation based on conversion after 14 h, absorbance at 400 nm (100× Kubelka Munk unit), and crystal structure of the exposed facets of BiOBr-001, BiOBr-010 and BiOBr-S-110.

less, despite the high adsorption of benzylamine at BiOBr-010, its specific productivity in mmol m$_{cat}^{-2}$ h^{-1} was lower than that of BiOBr-001 which suggests that adsorption does not play a major role in the photoactivity.

A contributing factor for the higher intrinsic activity of the (001)-facetted sample could be due to better charge separation between the electron-hole pairs. The layered structure of BiOX leads to a permanent dipole between the [Bi$_2$O$_2$]$^{2+}$ and X$^-$ slabs, resulting in the generation of an internal electric field. Upon photon absorption, electron-hole pairs are created in the bulk of the crystal. These electron–hole pairs separate under the influence of this internal electric field. For the {001}-oriented sample, the internal field is perpendicular to the facets and separation of charges occurs along the shortest crystal dimension which is the thickness of the platelets (Fig. S8). The internal field is aligned parallel in the {010}- and {110}-oriented crystals and the separated charges would have to diffuse over a larger distance of the width of the platelets.

The applicability of BiOBr for selective aerobic oxidation of different amines was examined (Table 3). While methyl sub-
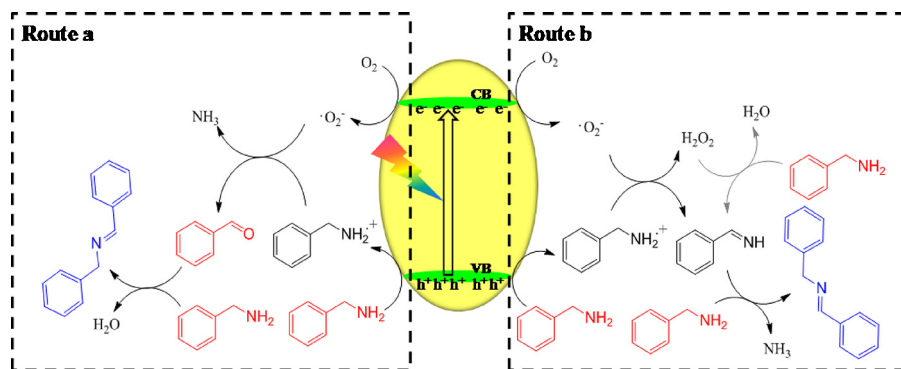
Scheme 2. Proposed reaction mechanisms for selective oxidation of benzylamine over BiOBr.

stituted benzylamines reached similarly high conversions as benzylamine, they differed in their selectivity. The selectivity to the *N*-benzylidenebenzylamines was 100% for the *meta*-substituted benzylamine, but decreased to 97 and 32% for the *ortho*- and *para*-substituted methylbenzylamines with formation of the corresponding aldehydes. Similarly, 100% yields of the *N*-benzylidenebenzylamines were observed for the *meta*-substituted methoxy and chloro benzylamines. In contrast, the *para*-substituted fluorobenzylamine had only 15 % selectivity to the *N*-fluorobenzylidenebenzylamine with major products being 4-fluorobenzaldehyde and 4-fluorobenzylimine. No reaction was observed for cyclohexylamine and butylamine. Dibenzylamine also afforded the corresponding secondary imine with 90.7% selectivity and aldehyde as by-product.

Upon visible light irradiation, electron-hole pairs are generated in BiOBr. The transfer of the electron from the conduction band to O_2 forms the superoxide $^\bullet O_2^-$ radical while oxidation of benzylamine by the holes forms the benzylammonium cation radical. There are two possible pathways for the formation of *N*-benzylidenebenzylamine from benzylamine. In one, the benzylammonium cation radical is oxidized by the $^\bullet O_2^-$ radical to phenylacetaldyde and NH_3 (Scheme 2, route a) [11]. The phenylacetaldyde undergoes condensation with another benzylamine to form the product. No phenylacetaldyde was observed in the oxidation of benzylamine although the formation of aldehydes was detected for some of the *o*-, *p*-substituted benzylamines where the reaction was slower. Hence, it is possible that the reaction occurs via this route as once the phenylacetaldyde is formed, it can react with benzylamine to form *N*-benzylidenebenzylamine, resulting in its concentration below detection limit. Indeed, this reaction was observed to occur rapidly upon mixing of phenylacetaldyde with benzylamine in the presence of BiOBr. Another route is via oxidative dehydrogenation of the benzylamine (Scheme 2, route b) [14,15]. Removal of hydrogen from the benzylammonium cation radical by the $^\bullet O_2^-$ radical forms the intermediate, benzylimine, and H_2O_2. Benzylimine then reacts with another molecule of benzylamine to form the final product, *N*-benzylidene benzylamine, releasing NH_3. We observed the presence of benzylimine as an intermediate during the reaction. Its concentration built up to a maximum at 5 h before decreasing with longer times (Fig. 6). Su et al. proposed that the coordination of benzylimine with a positively charged hole makes it more susceptible to a nucleophilic attack by benzylamine forming an aminal which then loses an NH_3 molecule to form the product [14]. The H_2O_2 formed in the dehydrogenation step goes on to oxidize another benzylamine to form benzylimine and water. We tested this possibility by using a mixture of H_2O_2 and benzylamine without any catalyst. However, no benzylimine was detected and after 14 h, only about 9.6% *N*-benzylidene benzylamine was formed (Table 2, entry 15). Based on the detection of aldehydes and ben-
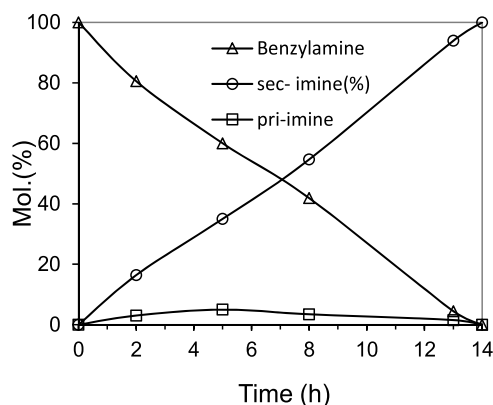

Fig. 6. Kinetic profile for selective aerobic oxidation of benzylamine using BiOBr-S-110.
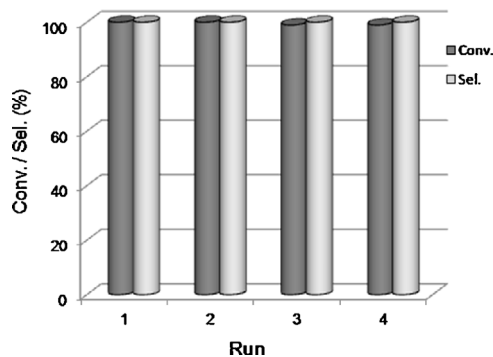

Fig. 7. Conversion and selectivity of recycled BiOBr-S-110.

zylimines as intermediates, both routes are possible in the selective oxidation of benzylamines.

After the photocatalytic reaction, BiOBr was filtered, washed with acetone and used for further batch reactions. The recycled photocatalyst retained its excellent conversion and selectivity for benzylamine oxidation even after 4 runs (Fig. 7), indicating the robust nature of this material. The x-ray diffractogram of the used catalyst was similar to that of the fresh sample (Fig. S9).

4. Conclusions

A systematic study was carried out on the selective photocatalytic oxidative coupling of amines to the corresponding secondary imines in the presence of bismuth oxyhalide photocatalysts. It was found that BiOBr exhibited excellent activity, with 100% conversion and selectivity after 14 h under visible light irradiation at room tem-

perature with oxygen from atmospheric air. The orientation of the exposed planes played a significant role in the photoactivity with the {001}-orientation having the highest intrinsic activity based on unit surface area. However, the BiOBr-{001} had a very low surface area in contrast to the solvothermally-synthesized BiOBr-S-110 microspheres which was composed of nanosheets with dominant {110} exposed facets. This latter sample exhibited high photoactivity for various benzylamines. *Meta*-substituted benzylamines were selectively oxidized to *N*-benzylidenebenzylamines with full conversion. Because of the convenient procedure using visible light from a normal light bulb, BiOBr can be considered as an environmental friendly, stable and reusable green photocatalyst for the synthesis of secondary imines which are obtained under mild reaction conditions in excellent conversion and selectivity. This work highlights the great potential of bismuth oxyhalides in the application of organic synthesis.

Acknowledgements

Appendix A. Supplementary data

Supplementary data associated with this article can be found, in the online version, at http://dx.doi.org/10.1016/j.apcatb.2017.07.050.

References

[1] S.I. Murahashi, Synthetic aspects of metal-catalyzed oxidations of amines and related reactions, Angew. Chem. Int. Ed. 34 (1995) 2443–2465.
[2] C.M. Silva, D.L. Siva, L.V. Modolo, R.B. Alves, M.A. Resende, C.V.B. Martins, A. Fatima, Schiff bases: a short review of their antimicrobial activities, J. Adv. Res. 2 (2011) 1–8.
[3] R.W. Layer, The chemistry of imines, Chem. Rev. 63 (1963) 489–510.
[4] M. Largeron, Protocols for the catalytic oxidation of primary amines to imines, Eur. J. Org. Chem. 24 (2013) 5225–5235.
[5] R. Tang, S.E. Diamond, N. Neary, F. Mares, Homogeneous catalytic oxidation of amines and secondary alcohols by molecular oxygen, J. Chem. Soc. Chem. Commun. 13 (1978) 562.
[6] A.J. Bailey, B.R. James, Catalysed aerobic dehydrogenation of amines and an X-ray crystal structure of a bis (benzylamine) ruthenium (II) porphyrin species, Chem. Commun. 20 (1996) 2343–2344.
[7] K. Yamaguchi, N. Mizuno, Efficient heterogeneous aerobic oxidation of amines by a supported ruthenium catalyst, Angew. Chem. Int. Ed. 42 (2003) 1480–1483.
[8] L. Aschwanden, T. Mallat, F. Krumeich, A. Baiker, A simple preparation of an efficient heterogeneous gold catalyst for aerobic amine oxidation, J. Mol. Catal. A: Chem. 309 (2009) 57–62.
[9] L. Aschwanden, T. Mallat, M. Maciejewski, F. Krumeich, A. Baiker, Development of a new generation of gold catalysts for amine oxidation, ChemCatChem 2 (2010) 666–673.
[10] M.H. So, Y. Liu, C.M. Ho, C.M. Che, Graphite-supported gold nanoparticles as efficient catalyst for aerobic oxidation of benzylic amines to imines and N-substituted 1, 2, 3, 4-tetrahydroisoquinolines to amides: synthetic applications and mechanistic study, Chem. Asian J. 4 (2009) 1551–1561.
[11] H. Lang, C. Ji, W. Chen, J. Ma, Zhao, Selective formation of imines by aerobic photocatalytic oxidation of amines on TiO$_2$, Angew. Chem. Int. Ed. 50 (2011) 3934–3937.
[12] B. Yang, X. Chen, Li Li, L. Zheng, C. Wu, Tung, Photocatalytic organic transformation by layered double hydroxides: highly efficient and selective oxidation of primary aromatic amines to their imines under ambient aerobic conditions, Chem. Commun. 50 (2014) 6664–6667.
[13] S. Furuawa, Y. Ohno, T. Shishido, K. Teramura, T. Tanaka, Selective amine oxidation using Nb$_2$O$_5$ photocatalyst and O$_2$, ACS Catal. 1 (2011) 1150–1153.
[14] F. Su, S.C. Mathew, L. Mohlmann, M. Antonietti, X. Wang, S. Blechert, Aerobic oxidative coupling of amines by carbon nitride photocatalysis with visible light, Angew. Chem. Int. Ed. 50 (2011) 657–660.
[15] W. Zhao, C. Liu, L. Cao, X. Yin, H. Xu, B. Zhang, Porous single-crystalline CdS nanosheets as efficient visible light catalysts for aerobic oxidative coupling of amines to imines, RSC Adv. 3 (2013) 22944–22948.
[16] S. Sarina, H. Zhu, E. Jaatinen, Q. Xiao, H. Liu, J. Jia, C. Chen, J. Zhao, Enhancing catalytic performance of palladium in gold and palladium alloy nanoparticles for organic synthesis reactions through visible light irradiation at ambient temperatures, J. Am. Chem. Soc. 13 (2013) 5793–5801.
[17] Z.J. Wang, S. Ghasimi, K. Landfesterand, K.A.I. Zhang, Molecular structural design of conjugated microporous poly (benzooxadiazole) networks for enhanced photocatalytic activity with visible light, Adv. Mater. 27 (2015) 6265–6270.
[18] J.H. Ko, N. Kang, N. Park, H.-W. Shin, S. Kang, S.M. Lee, H.J. Kim, T.K. Ahn, S.U. Son, Hollow microporous organic networks bearing triphenylamines and anthraquinones: diffusion pathway effect in visible light-driven oxidative coupling of benzylamines, ACS Macro Lett. 4 (2015) 669–672.
[19] S. Naya, K. Kimura, H. Tada, One-step selective aerobic oxidation of amines to imines by gold nanoparticle-loaded rutile titanium (IV) oxide plasmon photocatalyst, ACS Catal. 3 (2013) 10–13.
[20] S. Naya, T. Niwa, R. Negishi, H. Kobayashi, H. Tada, Multi-electron oxygen reduction by a hybrid visible-light-photocatalyst consisting of metal-oxide semiconductor and self-assembled biomimetic complex, Angew. Chem. 126 (2014) 14114–14117.
[21] N.M. Leonard, L.C. Wieland, R.S. Mohan, Applications of bismuth (III) compounds in organic synthesis, Tetrahedron 58 (2002) 8373–8397.
[22] O. Rohr, Bismuth–the new ecologically green metal for modern lubricating engineering, Ind. Lubr. Tribol. 54 (2002) 153–164.
[23] K. Zhang, C. Liu, F. Huang, C. Zheng, W. Wang, Study of the electronic structure and photocatalytic activity of the BiOCl photocatalyst, Appl. Catal. B-Environ. 68 (2006) 125–129.
[24] J. Jiang, K. Zhao, X. Xiao, L.S. Zhang, Synthesis and facet-dependent photoreactivity of BiOCl single-crystalline nanosheets, J. Am. Chem. Soc. 134 (2012) 4473–4476.
[25] J. Zhang, F. Shi, J. Lin, D. Chen, J. Gao, Z. Huang, X. Ding, C. Tang, Self-assembled 3-D architectures of BiOBr as a visible light-driven photocatalyst, Chem. Mater. 20 (2008) 2937–2941.
[26] W. Lin, X. Wang, Y. Wang, J. Zhang, Z. Lin, B. Zhang, F. Huang, Synthesis and facet-dependent photocatalytic activity of BiOBr single-crystalline nanosheets, Chem. Commun. (2014), http://dx.doi.org/10.1039/C3CC41498A.
[27] Xiao, W. Zhang, Facile synthesis of nanostructured BiOI microspheres with high visible light-induced photocatalytic activity, J. Mater. Chem. 20 (2010) 5866–5870.
[28] A. Han, J. Sun, X. Lin, C. Yuan, G.K. Chuah, S. Jaenicke, Influence of facets and heterojunctions in photoactive bismuth oxyiodide, RSC Adv. 5 (2015) 88298–88305.
[29] R. Li, F. Zhang, D. Wang, J. Yang, M. Li, J. Zhu, X. Zhou, H. Han, C. Li, Spatial separation of photogenerated electrons and holes among {010} and {110} crystal facets of BiVO$_4$, Nature. Commun. 4 (2013) 1432.
[30] M. Zhou, H.B. Wu, J. Bao, L. Liang, X.W.D. Lou, Y. Xie, Ordered macroporous BiVO$_4$ architectures with controllable dual porosity for efficient solar water splitting, Angew. Chem. Int. Ed. 52 (2013) 8579–8583.
[31] H. Fu, C. Pan, W. Yao, Y. Zhu, Visible-light-induced degradation of rhodamine B by nanosized Bi$_2$WO$_6$, J. Phys. Chem. B 109 (2005) 22432–22439.
[32] C. Zhang, Y. Zhu, Synthesis of square Bi$_2$WO$_6$ nanoplates as high-activity visible-light-driven photocatalysts, Chem. Mater. 17 (2005) 3537–3545.
[33] M. Muruganandham, R. Amutha, G.-J. Lee, S.-H. Hsieh, J.J. Wu, M. Sillanpaa, Facile fabrication of tunable Bi$_2$O$_3$ self-assembly and its visible light photocatalytic activity, J. Phys. Chem. C 116 (2012) 12906–12915.
[34] L. Zhou, W. Wang, H. Xu, S. Sun, M. Shang, Bi$_2$O$_3$ hierarchical nanostructures: controllable synthesis, growth mechanism, and their application in photocatalysis, Chem. Eur. J. 15 (2009) 1776–1782.
[35] R.A. Smith, Semiconductors, 2nd ed., Cambridge University Press, Cambridge, 1978.
[36] S. Higashimoto, Y. Hatada, R. Ishikawa, M. Azuma, Y. Sakata, H. Kobayashi, Selective photocatalytic oxidation of benzyl amine by O$_2$ into N-benzylidenebenzylamine on TiO$_2$ using visible light, Current. Org. Chem. 17 (2013) 2374–2381.
[37] M.A. Butler, D.S. Ginley, Prediction of flatband potentials at semiconductor-electrolyte interfaces from atomic electronegativities, J. Electrochem. Soc. 125 (1978) 228–232.